NOTES AND CORRESPONDENCE
Is the Antarctic Ozone Hole Recovering Faster than Changing the Stratospheric Halogen Loading?

Janusz KRZYŚCIN

Institute of Geophysics, Polish Academy of Sciences, Poland

(Manuscript received 29 February 2020, in final form 22 June 2020)

Abstract

A method is proposed to gain insight into ozone recovery over Antarctica. The following metrics relating to the ozone hole are considered: minimum total column ozone (TCO_3) within the hole, TCO_3 at the South Pole, area of the ozone hole, mass of ozone loss within the hole, and density of loss per unit area. The daily metric values, based on the Royal Netherlands Meteorological Institute archives of the ozone hole, are averaged for each year over the period 1979–2019 for the following intervals: 1–30 September, 15 September–15 October, 1–31 October, 15 October–15 November, and 1–30 November. The following indicators of the ozone hole recovery are examined: the metric recovery rate by 2019 (i.e., the change between its extreme and its 2019 level divided by the change between the extreme year and 1980) and the year of metric recovery. The recovery year is derived by forward-in-time extrapolation of the metric linear trend found for the period 2000–2019. The uncertainties in these indicators are obtained using a bootstrap approach analyzing statistics of the synthetic time series of the metrics. A comparison of the proposed ozone hole healing indicators with the indicators inferred from the equivalent effective stratospheric chlorine (EESC) loading over Antarctica (22.1 % and year 2076) shows to what extent recovery of the ozone layer is associated with EESC effects. For the mass and density of ozone loss in the periods 1–30 September and 15 September–15 October, the metric recovery rate by 2019 is ~ 2 times larger and the recovery year is at least 20–30 years earlier than the corresponding indicators of the EESC changes. Therefore, the ozone hole is recovering faster during these periods than expected based on the stratospheric halogen loading alone.

Keywords ozone hole; Antarctica; halogens; recovery

Citation Krzyścin, J., 2020: Is the Antarctic ozone hole recovering faster than changing the stratospheric halogen loading. *J. Meteor. Soc. Japan*, **98**, 1083–1091, doi:10.2151/jmsj.2020-055.

1. Introduction

A large deficit in stratospheric ozone has appeared over Antarctica in every Austral spring since the beginning of the 1980s. The first report on extreme low ozone content over Antarctica came from total column ozone (TCO_3) observations made by Dr. Shigeru Chubachi at the Japanese Antarctic station Syowa in 1982 (Chubachi 1984). It was later found that satellite TCO_3 data from the early 1980s also indicated an ozone deficit; however, at that time, such low TCO_3 values were disregarded as instrumental error (Stolarski et al. 1986). Farman et al. (1985) found that the extremely low ozone over Antarctica had a chemical origin related to the activation of inorganic chlorine in the stratosphere.

Worldwide interest in the ozone hole over Ant-

Corresponding author: Janusz Krzyścin, Institute of Geophysics, Polish Academy of Sciences, Ks. Janusza 64 Street, Warsaw, 01-452, Poland
E-mail: jkrzys@igf.edu.pl
J-stage Advance Published Date: 25 August 2020

arctica led to the signing of the 1987 International Agreement, the Montreal Protocol (MP), which restricted the production and use of the substances most hazardous to the ozone layer, i.e., anthropogenic halocarbons containing chlorine and bromine. Observations of long-term changes in concentrations of both chlorine- and bromine-containing gases in the Antarctic troposphere showed a peak around the mid-1990s (Montzka et al. 2019). The application of chemistry–climate models indicated that the concentration maximum of these substances occurred around 2001–2002 in the Antarctic stratosphere (Montzka et al. 2019). Since then, a slow healing of Antarctic ozone has been expected owing to the long residence time of some highly reactive stratospheric halocarbons, which may be several decades (World Meteorological Organization 2014, 2018).

Ozone variability inside the Antarctic vortex can be attributed to both the changing concentration of ozone-depleting substances (ODS) in the stratosphere and dynamical variability influencing ozone chemistry (e.g., stratospheric temperature changes affecting chemical reactions and the appearance of polar stratospheric clouds in the cold polar vortex) and the transport of ozone and substances indirectly affecting ozone (e.g., volcanic aerosols).

Equivalent effective stratospheric chlorine (EESC) provides an estimate of the stratosphere loading of ODSs and has been frequently used for estimations of man-made ozone depletion. EESC values are calculated from ODS emissions into the troposphere and modeled transport into the lower stratosphere (Newman et al. 2007).

An overturning of the trend in Antarctic ozone around 2000 has been identified (Yang et al. 2008; Salby et al. 2011). Evidence of Antarctic ozone recovery has been discussed in many papers (e.g., Kuttippurath and Nail 2017; de Laat et al. 2017; and Pazmiño et al. 2018). Analysis of the observed and modeled ozone data by Solomon et al. (2016) indicated that the onset of Antarctic ozone healing could be clearly seen in September and could be confidently linked to the anthropogenic halogen changes forced by the 1987 MP and its subsequent amendments. Kuttippurath et al. (2018a) showed a reduction in the occurrence of ozone loss saturation in the stratosphere (~ 13–21 km), supporting the emergence of ozone recovery occurring after the peak in ODS concentration over Antarctica.

Various metrics for monitoring the ozone hole are possible, including: minimum TCO_3 within the hole, TCO_3 at the South Pole, area of the ozone hole with $TCO_3 < 220$ DU, and mass of ozone loss (difference between actual TCO_3 and 220 DU integrated over the hole area).

Herein, are proposed indicators of ozone hole recovery applied to the above-mentioned metrics, i.e., the metric recovery rate by 2019 (i.e., the change between its extreme and its 2019 level divided by the change between the extreme year and 1980), and the year of the metric recovery (the time when the metric value returned to its initial 1980 value).

The novelty of this paper stems from analyzing ozone recovery over Antarctica in terms of the proposed indicators for the metrics of the ozone hole and their relation to the indicators derived from the EESC loading over Antarctica. A comparison between the metrics and EESC indicators will reveal if the ozone recovery inferred from the metric recovery rate by 2019 is larger, and the recovery year earlier, than the corresponding EESC values.

2. Materials and methods

2.1 Ozone hole metrics and healing indicators

The Royal Netherlands Meteorological Institute (KNMI) has archived ozone hole status since 1979 using the following daily metrics: TCO_3 minimum within the hole (*i*), TCO_3 at the South Pole (*ii*), area of $TCO_3 < 220$ DU (*iii*), and mass of ozone loss (*iv*). In addition, herein, a new metric is proposed, i.e., the density of the ozone loss per unit area of the hole (*v*).

Annual files of the daily metric values are available at the web page http://www.temis.nl/protocols/o3hole/o3_history.php?lang=0. These values were extracted from the multi-sensor reanalysis (MSR) data comprising corrected (for instrumental drift) and calibrated (against ground-based observations by the Dobson and Brewer spectrophotometers) TCO_3 values from various satellite measurements including TOMS, SBUV, GOME, SCIAMACHY, OMI, and GOME-2 (van der A et al. 2015).

To monitor the present (2019) status of the Antarctic ozone hole and its recovery time, the following ozone hole healing indicators (HI) calculated for all metrics are considered: the metric recovery rate by 2019, $HI_{R,\,2019}$ (the change between the extreme value of the metric and its value in 2019, expressed as the percentage change between the metric extreme and its value in 1980), and the metric recovery year, HI_{Year} (i.e., the time when the metric value reaches its initial 1980 value; 220 DU for metrics *i* and *ii*, or zero for other metrics). $HI_{R,\,End} = 100$ % indicates full recovery of the metric value at the end of the time series (End) equal to the value at the beginning (1980). The recov-

ery year is derived by forward-in-time extrapolation of the straight line found by the linear least-squares fit of the 2000–2019 metric values.

2.2 Proxies of the ozone variabilities

EESC time series over Antarctica provided by Montzka et al. (2019) were used. It was assumed that 5.5 years is the "mean age" for halogens in the stratosphere and that the ozone depleting efficiency of inorganic bromine is 60 times larger than that of chlorine compounds. Montzka et al. (2019) proposed the ozone depleting gas index to monitor ODS decline and found that 22.1 % of the stratospheric ODS over Antarctica had been recovered by 2019. Forward-in-time extension of the EESC linear pattern in the 2000–2019 period yielded a recovery year of 2076 for an ODS level equal to the 1980 level. We follow their approach in Section 2.1, defining the ozone hole healing indicators based on the metric changes.

Dynamical proxies are related to known processes affecting ozone variability such as solar activity, the poleward eddy heat flux, volcanic aerosols in the stratosphere, the quasi-biennial oscillation, El Niño–Southern Oscillation, and the Antarctic Oscillation. This set of proxies has been commonly used in previous statistical models of ozone variability (e.g., Pazmiño et al. 2018; Krzyścin and Baranowski 2019). The time series of the dynamical proxies were taken from the same web sites used in our previous paper (Krzyścin and Baranowski 2019).

2.3 Uncertainties of the ozone hole healing indicators

Bootstrapping was used to determine the sensitivity of $HI_{(...)}$ estimates with respect to year-to-year variations in the metrics. A large sample ($N = 10{,}000$) of synthetic time series of the annual metric values for the period 1979–2019 was generated to determine the statistical characteristics of the $HI_{(...)}$ sample, i.e., the median and the 95 % confidence interval (2.5th–97.5th percentile range). The following multi-step algorithm is proposed to generate the synthetic time series of the metric for the period 1979–2019:

a) from the original K-th metric time series, $MET_K(t)$, the smoothed pattern of $\langle MET_K(t)\rangle$ and the corresponding residuals, $MET'_K(t)$, are extracted by the locally weighted scatterplot smoothing (LOWESS) (Cleveland 1979), i.e., $MET_K(t) = \langle MET_K(t)\rangle + MET'_K(t)$.
b) the randomness of $MET'_K(t)$ values, $t = \{1979, \ldots., 2019\}$ is assessed by the Wald–Wolfowitz test of randomness (Wald and Wolfowitz 1943). The algorithm proceeds to the next step if the test is fulfilled; if not, a random portion of the residuals is extracted using an autoregressive model
c) random drawing with replacement is applied to the $MET'_K(t)$ values to build the n-th synthetic time series of the metric residuals, $MET'_{K,n}(t)$, $n = \{1, \ldots, N = 10{,}000\}$, $t = \{1979, \ldots. , 2019\}$
d) The Wald–Wolfowitz runs test (Wald and Wolfowitz 1940) is used to determine if the $MET'_{K,n}(t)$ and original $MET'_K(t)$ have the same distribution. Only a $MET'_{K,n}(t)$ series passing the test is used in the next step
e) A synthetic representative of the original time series of the K-th metric is built by adding $MET'_{K,n}(t)$ to the original smoothed pattern of the K-th metric:

$$MET_{K,n}(t) = \langle MET_K(t)\rangle + MET'_{K,n}(t).$$

f) a smooth component of the synthetic time series, $\langle MET_{K,n}(t)\rangle$, built in step e, is extracted by the LOWESS smoother and used in calculations of the synthetic $HI_{(...)}$ values for K-th metric, the metric recovery rate by 2019, $HI_{R,\,2019,\,K,\,n}$, and the recovery year, $HI_{Year,\,K,\,n}$.
g) by repeating steps c–f many times, a sample of the synthetic $HI_{(...)}$ values is created: $\{HI_{R,\,2019,\,K,\,n}, HI_{Year,\,K,\,n}, K = 1, \ldots, 5$, and $n = 1, \ldots, 10{,}000\}$.
h) the median, 2.5th percentile, and 97.5th percentile are calculated from the ordered (from lowest to highest) values of the sample obtained in step g.

Two versions of the algorithm were implemented. The first is described above. In the second version, after step a, a standard multivariate regression model, with the proxies defined in Section 2.2, was applied to the $MET'_K(t)$ time series to identify the portion of metric variability resulting from the parameterized dynamical processes. The dynamical signal was subtracted from the residuals and the next steps were applied to the residuals with the "natural" variability removed.

3. Results and discussion

The usefulness of satellite data for monitoring ozone long-term variability over southern high latitudes is already known (Kuttippurath et al. 2018b; Krzyścin and Baranowski 2019). This can also be demonstrated by a comparison of the metric *ii* values (TCO_3 over the South Pole) with TCO_3 from ground-based observations at the Amundsen–Scott SP station (Fig. 1a). In spite of the large intra-month variability of TCO_3 (uncertainty bars in Fig. 1b), the smoothed patterns of the modeled and observed ozone values look very similar, with a maximum difference between the curves of ~ 5 DU (2–3 %) (Fig. 1b).

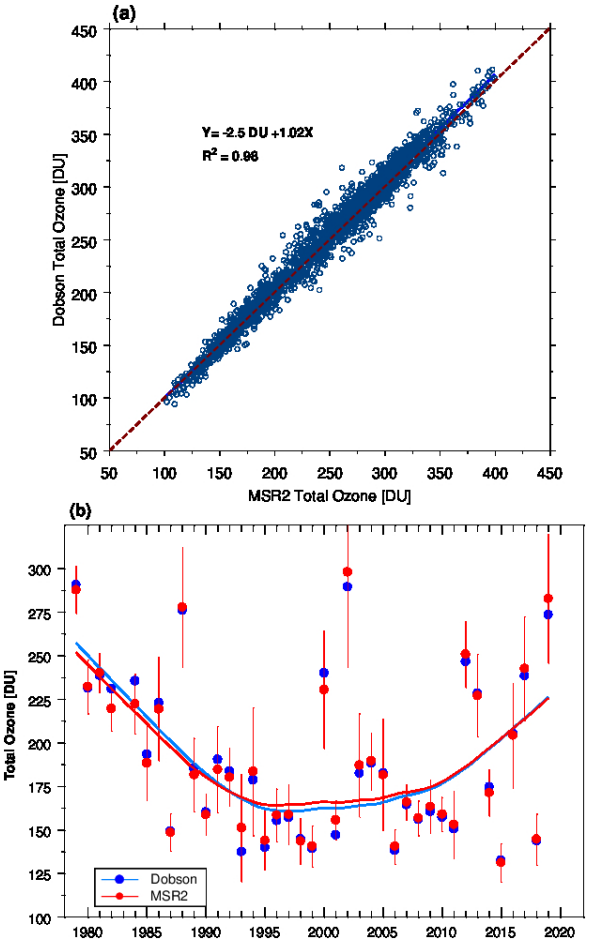

Fig. 1. Daily total column ozone values from the Dobson spectrophotometer measurements at the South Pole versus corresponding MSR total column ozone (a), time series (1979–2019) of the mean total ozone over the period 15 September to 15 October from the ground-based measurements at the South Pole and MSR data (b). The solid lines show the smoothed profiles by the LOWESS filter. Vertical lines represent uncertainty ranges of the mean total column ozone.

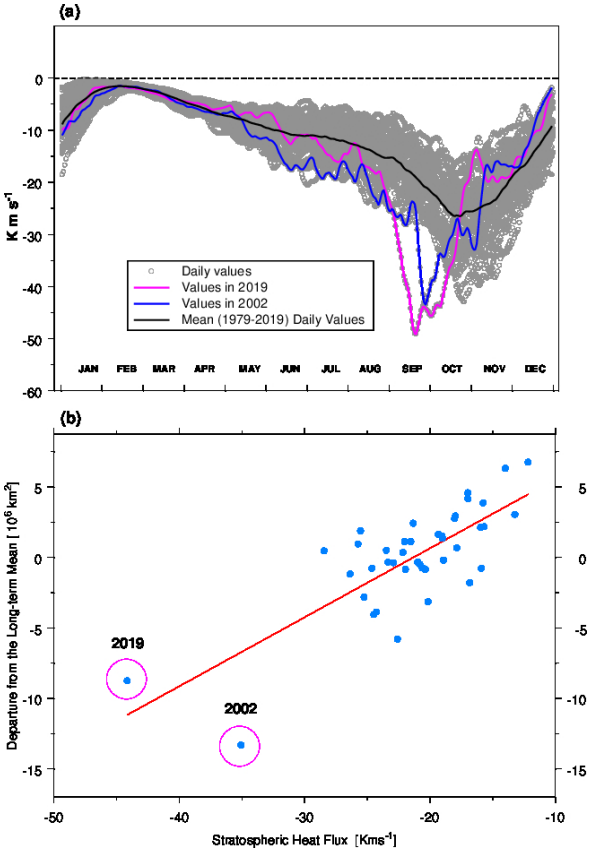

Fig. 2. Time series of the 45-day mean heat flux between 45°S and 75°S at 50 hPA, from the MERRA-2 reanalysis, wherein the black curve shows the smoothed pattern of this series and the extreme yearly series are for 2002 (blue curve) and 2019 (violet curve) (a). Departures of the hole area in the 15 September–15 October period from it's long-term (1979–2019) mean value versus the corresponding heat flux (b).

The extreme large poleward heat flux has a large impact on the metric values, as warming of the Antarctic atmosphere lowers the amount of polar stratospheric clouds (PSC) generated. Here, the 45-day average of the heat flux lag prior the TCO_3 date was used as there was a stronger anticorrelation (−0.61) between it and the stratospheric temperature over Antarctica, as compared with the case for the non-lagged heat flux.

The presence of PSC in the Antarctic stratosphere is decisive in terms of ozone loss rate (Solomon et al. 1986). A high degree of heating of the Antarctic stratosphere at the end of the winters of 2002 and 2019 (Fig. 2a) led to a reduction in the hole size of about 10 M km^2 during 15 September–15 October (Fig. 2b). The warm air present in the Antarctic stratosphere in these extreme years was forced by a sudden stratospheric warming (SSW), which is a rare phenomenon over Antarctica (as compared with the Arctic) (Lim et al. 2020). Including these two years in a statistical analysis of the hole variability increases the uncertainty ranges discussed in Section 2.3. However, we decided to retain these anomalies in the bootstrapping procedure to account for the possibility of such ex-

treme disturbances in the Antarctic dynamics.

Figure 3b–e shows an example of the analyzed time series of the metrics for September. Moreover, the EESC time series over Antarctica, i.e., a basic driver of the long-term hole variability, is presented in Fig. 3a. The metric values are smoothed by the LOWESS filter to delineate their long-term variability. The scale of the smoothing is selected ($f = 0.5$ in the LOWESS filter) to have the same quasi-parabolic shape of the smoothed metric pattern as in the original EESC series.

Values of the ozone hole healing indicators are embedded into Fig. 3. It is seen that for all metrics, the recovery seems to be faster than that observed in the EESC series. For example, the recovery years of 2034 and 2076 are observed in Figs. 3e and 3a, respectively. However, a large year-to-year variability in the metric values, especially after year 2000, should be taken into account to determine if these differences are statistically significant.

Table 1 shows estimates (median and the 95 % uncertainty range) of the $HI_{(...)}$ values calculated for the metric data averaged over the following overlapping periods: 1–30 September, 15 September–15 October, 1–31 October, 15 October–15 November, and 1–30 November. In addition, the linear trend values of the metrics for the period 2000–2019 are shown to provide the recovery years using the forward-in-time extrapolation of the regression line found in the 2000–2019 data. The results are derived from 10,000 samples of the synthetic $HI_{(...)}$ values (Section 2.3). Residual fluctuations due to dynamic proxies are not removed from the residual series because the residuals themselves were found to represent random noise for all metrics considered. However, the results for the model version accounting for the dynamical proxies (not shown in Table 1) will be discussed further.

Uncertainty ranges for all $HI_{R,\ 2019,\ K}$ values do not contain zeros for the periods 1–30 September. and 15 September–15 October. This indicates a pseudo-parabolic pattern of the smoothed metric series, with the maximum (metrics *iii*, *iv*, and *v*) or the minimum (metrics *i* and *ii*) values within the 1979–2019 period. Cases with an uncertainty range containing zero appear later, i.e., October and November. This indicates that a monotonic change exists throughout the whole period (no trend overturning) or a trendless pattern appears after the extreme year. However, overturning of the trend at some point during 1979–2019 could be claimed for all metrics if the natural variability is removed from the residuals.

The metric trends for the period 2000–2019 are statistically significant (the values of the 95 % range have the same sign) in 48 % of the combinations of the metric type (5 types possible) and period (5 periods possible). All metric types yielded statistically significant trends in September for all years from 2000 to 2019; these were increasing trends for metrics *i* and *ii* and decreasing trends for the other metrics. Statistically significant trend value translates into the recovery year, $HI_{Year,\ K}$. The recovery year is somewhere between 2026 (metric *ii*, 1–30 September) and 2077 (metric *i*, 15 September–15 October). The earliest recovery (~ 2030) with the smallest uncertainty range (20–30 years) is envisaged for metrics *iv* and *v* (i.e., ozone loss in the hole and density of the loss, respectively) in September. For other periods, the uncertainty of the recovery year estimate increased and the recovery year showed the potential to increase beyond 2100.

Using the synthetic metrics with the parameterized effects by the dynamical proxies only slightly changed the median value and the 95 % confidence interval. The median of the recovery year varied by a maximum of several years. For some metrics, the uncertainty was potentially in the range of ~ 5–10 years shorter, or even longer. Such variability did not change the general interpretation of the state of the ozone hole in 2019 or the envisaged date of its recovery.

Long-term ozone hole variability is strongly affected by EESC changes. Therefore, it was considered interesting to determine how the metric $HI_{(...)}$ values (shown in Table 1) corresponded with the indicators ($HI_{R,\ 2019,\ EESC}$ and $HI_{Year,\ EESC}$) inferred from the EESC time series. The following values were obtained: $HI_{R,\ 2019,\ EESC} = 22.1$ %, $HI_{Year,\ EESC} = 2076$ (Fig. 3a). Such measures are outside the uncertainty ranges for certain metrics (values in bold font in Table 1); for example, this occurs for metrics *iv* and *v* in the following periods: 1–30 September, 15 September–15 October, and 15 October–15 November. In these cases, the median of the metric recovery rate by 2019 is ~ 2 times larger than the corresponding value inferred from the EESC time series. Moreover, in September, the recovery year for metrics *iv* and *v* is significantly earlier (at least 20 years) than the year (2076) that the EESC returned to its 1980 value (Fig. 3 a).

The recovery year, derived from the envisaged EESC changes, was also calculated with substantial uncertainty because of approximations of various characteristics of halogen concentrations in the stratosphere (e.g., mean age-of-air and fractional halogen release values). Newman et al. (2007) derived an EESC recovery year of 2067, with a 95 % confidence

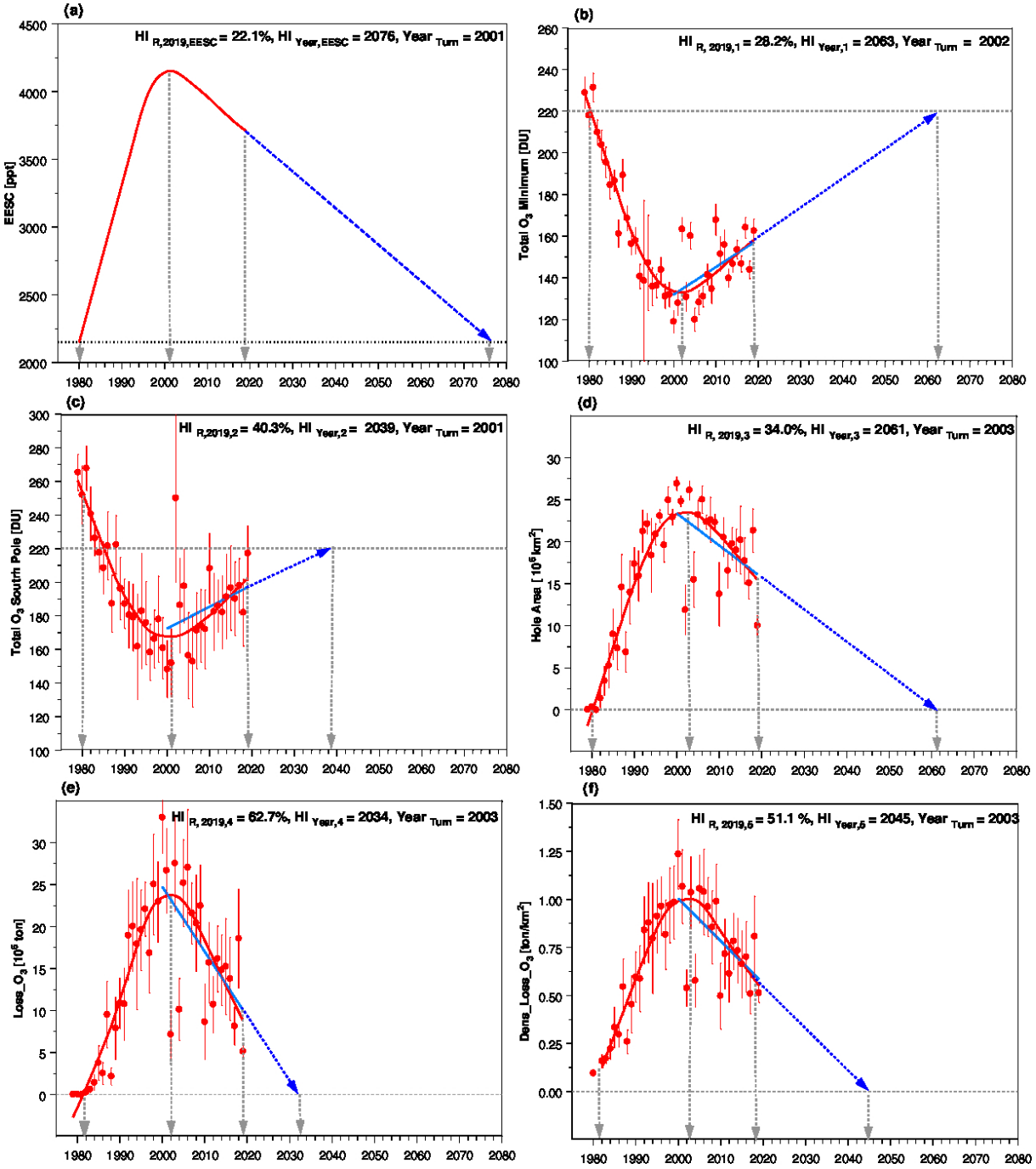

Fig. 3. Time series of EESC over Antarctica with the regression line fit to the 2000–2019 EESC yearly data (a). The metric time series (red points) in September and the linear trends in the period 2000–2019 (blue solid lines) are for the minimum of total column ozone within the hole (b), total column ozone at the South Pole (c), ozone hole area (d), mass of ozone loss within the hole (e), and density of loss per km^2 (f). The straight lines (blue dashed lines) are extended until they reach the initial (1980) value (arrow head). The smoothed curves (red) represent the smoothed values by the LOWESS filter. Values of the ozone hole healing indicators, $HI_{(...)}$, together with the trend overturning year, $Year_{Turn}$, are embedded into the figures. Vertical lines represent the uncertainty ranges of the metric values.

Table 1. Median, linear trend in the 2000–2019 period, and 95th confidence range of the ozone hole healing indicator, $HI_{(...)}$, estimates for the following metrics: the minimum total ozone within the hole (MET_1), total column ozone at the South Pole (MET_2), area of the ozone hole (MET_3), mass of ozone loss within the hole (MET_4), and density of loss per km^2 (MET_5). The results are for the following periods: 1–30 September, 15 September–15 October, 1–31 October, 15 October–15 November, and 1–30 November. Bold font marks $HI_{(...)}$ estimates that were significantly different to the corresponding indicators derived from the EESC series ($HI_{R,\,2019,\,EESC} = 22.1$ % and $HI_{Year,\,EESC} = 2076$). Add 2000 to the recovery year shown in column $HI_{Year,\,K}$.

Metrics	Value	$HI_{R,\,2019,\,K}$ (%)	Trend (2000–2019) (Value $year^{-1}$)	$HI_{Year,\,K}$ (year)
		1–30 September		
MET_1	DU	24.1 (13.2, 38.1)	1.43 (0.54, 2.32)	59 (37, 143)
MET_2	DU	35.1 (19.7, 52.3)	1.96 (0.49, 3.41)	26 (15, 98)
MET_3	M km^2	29.3 (18.0, 43.9)	−0.46 (−0.72, −0.18)	50 (33, 120)
MET_4	M t	**55.2** (40.8, 76.0)	−0.85 (−1.20, −0.49)	**26** (19, 43)
MET_5	t km^{-2}	**49.5** (34.4, 67.5)	−.031 (−.046, −.016)	**32** (22, 59)
		15 September–15 October		
MET_1	DU	21.4 (10.2, 35.3)	1.34 (0.37, 2.35)	77 (42, 239)
MET_2	DU	22.7 (11.2, 38.0)	1.51 (−0.31, 3.46)	N/A
MET_3	M km^2	14.6 (0.9, 28.7)	−0.21 (−0.50, 0.01)	N/A
MET_4	M t	**41.5** (24.1, 64.4)	−0.83 (−1.29, −0.34)	35 (24, 79)
MET_5	t km^{-2}	**37.8** (25.6, 50.8)	−.030 (−.046, −.013)	43 (28, 97)
		1–31 October		
MET_1	DU	18.2 (0.9, 36.4)	−0.87 (−0.33, 2.12)	N/A
MET_2	DU	10.8 (0.0, 48.3)	−0.72 (−0.97, 2.68)	N/A
MET_3	M km^2	19.3 (0.0, 40.6)	−0.22 (−0.51, 0.09)	N/A
MET_4	M t	41.4 (19.3, 63.5)	−0.62 (−1.09, −0.15)	40 (23, 141)
MET_5	t km^{-2}	29.4 (10.4, 52.3)	−.017 (−.034, .002)	N/A
		15 October–15 November		
MET_1	DU	28.3 (6.2, 54.8)	1.28 (−0.20, 2.63)	N/A
MET_2	DU	54.5 (18.9, 106.)	2.33 (−0.44, 4.96)	N/A
MET_3	M km^2	29.3 (0.6, 60.5)	−0.26 (−0.59, 0.01)	N/A
MET_4	M t	**59.2** (22.1, 95.2)	−0.54 (−1.00, −0.08)	31 (17, 139)
MET_5	t km^{-2}	**49.4** (22.8, 81.6)	−.021 (−.041, −.002)	43 (21, 191)
		1–30 November		
MET_1	DU	46.8 (17.7, 86.8)	2.08 (0.29, 4.05)	28 (15, 122)
MET_2	DU	68.1 (13.2, 175.)	3.13 (−0.58, 7.07)	N/A
MET_3	M km^2	48.6 (0.0, 125.)	−0.26 (−0.55, 0.07)	N/A
MET_4	M t	67.6 (0.0, 125.)	−0.29 (−0.60, 0.01)	N/A
MET_5	t km^{-2}	61.4 (0.0, 192.)	−.012 (−.047, .020)	N/A

interval from 2056 to 2078. It is worth mentioning that the 95 % confidence interval for the recovery year of metric *iv* in September is outside the range calculated by Newman et al. (2007). Therefore, relative to the year that the EESC returned to its 1980 value, an earlier recovery could be expected for this metric. It is assumed here that the stratospheric halogen loading will decrease at the rate found for the last two decades, i.e., that the regulations from the 1987 MP (and subsequent amendments) will function in the same manner in the future. However, Montzka et al. (2018) found a surprising increase in CFC-11 emissions in the Northern Hemisphere, and Dhomse et al. (2019) estimated that a continuation of this CFC-11 trend will significantly delay ozone hole recovery.

Simulations of TCO_3 at SP using a chemistry–climate model (Solomon et al. 2016) showed that a significant portion of the 2000–2014 trend in September was due to non-EESC forcing, i.e., the increase of 1.3 DU $year^{-1}$ was due to chemical forcing alone,

whereas the 1.9 DU year^{-1} value was due to combined chemical and dynamical forcing (see their Table S3). The ratio between those trend values was 1.46, which is close to the ratio of 1.59 found between the combined dynamical/chemical effects on TCO_3 at SP ($HI_{R,\ 2019,\ 2} = 35.1$ %, Table 1) and that due to stratospheric halogens only ($HI_{R,\ 2019,\ EESC} = 22.1$ %), as found herein for September 2019. This agreement between estimates confirms the usefulness of the proposed method for monitoring the ozone hole.

4. Conclusions

Herein, a new method for monitoring Antarctic ozone hole recovery has been proposed. Several metrics of the hole are examined: the minimum TCO_3 over Antarctica, TCO_3 at SP, area of the ozone hole with $TCO_3 < 220$ DU, mass of ozone loss inside the hole, and the density of the loss per unit area. The recovery of the ozone hole is discussed using indicators of the long-term variability in the metrics for various sub-periods in the 1 September–15 November period, i.e., metric recovery rate by 2019 and recovery year based on forward-in-time extension of the linear trend found for the period 2000–2019.

A comparison with the corresponding indicators, retrieved from the EESC time series, allows inference of the rate of ozone healing due to combined chemical and dynamical drivers. The most pronounced signal of recovery could be identified in the September and 15 September–15 October data for the mass and density of ozone loss in the hole. The metric recovery rate by 2019 for these metrics is about two times larger than that calculated from the EESC changes, and the recovery year will be at least 20–30 years earlier. Therefore, the Antarctic ozone hole is recovering faster at the end of the Austral winter and early spring than is expected based on the stratospheric halogen loading only.

Acknowledgments

This article was supported in the scope of the statutory activity No.3841/E-41/2020 of the Ministry of Science and Higher Education of Poland and by the Polish National Agency for Academic Exchange No. PPI/PZA/2019/1/00107/U/00001.

References

Chubachi, S., 1984: Preliminary result of ozone observations at Syowa from February 1982 to January 1983. *Mem. Natl Inst. Polar Res.*, **34**, 13–19.

Cleveland, W. S., 1979: Robust locally weighted regression and smoothing scatterplots. *J. Am. Stat. Assoc.*, **74**, 829–836.

de Laat, A. T. J., M. van Weele, and R. J. van der A, 2017: Onset of stratospheric ozone recovery in the Antarctic ozone hole in assimilated daily total ozone columns. *J. Geophys. Res.: Atmos.*, **122**, 11880–11899.

Dhomse, S. S., W. Feng, S. A. Montzka, R. Hossaini, J. Keeble, J. A. Pyle, J. S. Daniel, and M. P. Chipperfield, 2019: Delay in recovery of the Antarctic ozone hole from unexpected CFC-11 emissions. *Nat. Commun.*, **10**, 5781, doi:10.1038/s41467-019-13717-x.

Farman, J. C., B. G. Gardiner, and J. D. Shanklin, 1985: Large losses of total ozone in Antarctica reveal seasonal ClO_x/NO_x interaction. *Nature*, **315**, 207–210.

Krzyścin, J. W., and D. Baranowski, 2019: Signs of the ozone recovery based on multi sensor reanalysis of total ozone for the period 1979–2017. *Atmos. Environ.*, **199**, 334–344.

Kuttippurath, J., and P. J. Nair, 2017: The signs of Antarctic ozone hole recovery. *Sci. Rep.*, **7**, 585, doi:10.1038/s41598-017-00722-7.

Kuttippurath, J., P. Kumar, P. J. Nair, and P. C. Pandey, 2018a: Emergence of ozone recovery evidenced by reduction in the occurrence of Antarctic ozone loss saturation. *npj Climate Atmos. Sci.*, **1**, 42, doi:10.1038/s41612-018-0052-6.

Kuttippurath, J., P. Kumar, P. J. Nair, and A. Chakraborty, 2018b: Accuracy of satellite total column ozone measurements in polar vortex conditions: Comparison with ground-based observations in 1979–2013. *Remote Sens. Environ.*, **209**, 648–659.

Lim, E.-P., H. H. Hendon, A. H. Butler, R. D. Garreaud, I. Polichtchouk, T. G. Shepherd, A. Scaife, R. Comer, L. Coy, P. A. Newman, D. W. J. Thompson, and H. Nakamura, 2020: The 2019 Antarctic sudden stratospheric warming. *SPARC Newsl.*, **54**, 10–13.

Montzka, S. A., G. S. Dutton, P. Yu, E. Ray, R. W. Portmann, J. S. Daniel, L. Kuijpers, B. D. Hall, D. Mondeel, C. Siso, J. D. Nance, M. Rigby A. J. Manning, L. Hu, F. Moore, B. R. Miller, and J. W. Elkins, 2018: An unexpected and persistent increase in global emissions of ozone-depleting CFC-11. *Nature*, **557**, 413–417.

Montzka, S. A., G. Dutton, and J. H. Butler, 2019: *The NOAA Ozone Depleting Gas Index: Guiding recovery of the ozone layer*. NOAA Earth System Research Laboratory. [Available at https://www.esrl.noaa.gov/gmd/odgi/.]

Newman, P. A., J. S. Daniel, D. W. Waugh, and E. R. Nash, 2007: A new formulation of equivalent effective stratospheric chlorine (EESC). *Atmos. Chem. Phys.*, **7**, 4537–4552.

Pazmiño, A., S. Godin-Beekmann, A. Hauchecorne, C. Claud, S. Khaykin, F. Goutail, E. Wolfram, J. Salvador, and E. Quel, 2018: Multiple symptoms of total ozone recovery inside the Antarctic vortex during austral spring. *Atmos. Chem. Phys.*, **18**, 7557–7572.

Salby, M., E. Titova, and L. Deschamps, 2011: Rebound

of Antarctic ozone. *Geophys. Res. Lett.*, **38**, L09702, doi:10.1029/2011GL047266.

Solomon, S., R. R. Garcia, F. S. Rowland, and D. J. Wuebbles, 1986: On the depletion of Antarctic ozone. *Nature*, **321**, 755–758.

Solomon, S., D. J. Ivy, D. Kinnison, M. J. Mills, R. R. Neely III, and A. Schmidt, 2016: Emergence of healing in the Antarctic ozone layer. *Science*, **353**, 269–274.

Stolarski, R. S., A. J. Krueger, M. R. Schoeberl, R. D. McPeters, P. A. Newman, and J. C. Alpert, 1986: Nimbus 7 satellite measurements of the springtime Antarctic ozone decrease. *Nature*, **322**, 808–811.

van der A, R. J., M. A. F. Allaart, and H. J. Eskes, 2015: Extended and refined multi sensor reanalysis of total ozone for the period 1970–2012. *Atmos. Meas. Tech.*, **8**, 3021–3035.

Wald, A., and J. Wolfowitz, 1940: On a test whether two samples are from the same population. *Ann. Math. Stat.*, **11**, 147–162.

Wald, A., and J. Wolfowitz, 1943: An exact test for randomness in the non-parametric case based on serial correlation. *Ann. Math. Stat.*, **14**, 378–388.

World Meteorological Organization, 2014: *Scientific assessment of ozone depletion: 2014*. Global Ozone Research and Monitoring Project–Report No. 55, World Meteorological Organization, Geneva, 416 pp.

World Meteorological Organization, 2018: *Scientific assessment of ozone depletion: 2018*. Global Ozone Research and Monitoring Project–Report No. 58, World Meteorological Organization, Geneva, 588 pp.

Yang, E.-S., D. M. Cunnold, M. J. Newchurch, R. J. Salawitch, M. P. McCormick, J. M. Russell III, J. M. Zawodny, and S. J. Oltmans, 2008: First stage of Antarctic ozone recovKuttery. *J. Geophys. Res.*, **113**, D20308, doi:10.1029/2007JD009675.